The Jormungand global climate state and implications for Neoproterozoic glaciations

Dorian S. Abbot,[1] Aiko Voigt,[2] and Daniel Koll[1]

Received 7 March 2011; revised 11 June 2011; accepted 20 June 2011; published 17 September 2011.

[1] Geological and geochemical evidence can be interpreted as indicating strong hysteresis in global climate during the Neoproterozoic glacial events (~630 Ma and ~715 Ma). Standard climate theory only allows such strong hysteresis if global climate enters a fully-glaciated "Snowball" state. However, the survival of photosynthetic, eukaryotic, marine species through these glaciations may indicate that there were large areas of open ocean. A previously-proposed "Slushball" model for Neoproterozoic glaciations could easily explain the survival of these organisms because it has open ocean throughout the tropics, but there is only a small amount of hysteresis associated with the Slushball state. In this paper a new state of global climate, the "Jormungand" state, is proposed. In this state the ocean is very nearly globally ice-covered, but a very small strip of the tropical ocean remains ice-free. The low ice latitude of the Jormungand state is a consequence of the low albedo of snow-free (bare) sea ice. If the ice latitude propagates into the subtropical desert zone, it can stabilize without collapsing to the equator because subtropical ice-covered regions have a relatively low top-of-atmosphere albedo as a result of the exposure of bare sea ice and relatively lower cloud cover. Moreover, there is strong hysteresis associated with the Jormungand state as greenhouse gas levels are varied because of the high albedo contrast between regions of bare and snow covered sea ice. The Jormungand state is illustrated here in two different atmospheric global climate models and in the Budyko-Sellers model. By offering a scenario that could explain both strong hysteresis in global climate and the survival of life, the Jormungand state represents a potential model for Neoproterozoic glaciations, although further study of this issue is needed.

Citation: Abbot, D. S., A. Voigt, and D. Koll (2011), The Jormungand global climate state and implications for Neoproterozoic glaciations, *J. Geophys. Res.*, *116*, D18103, doi:10.1029/2011JD015927.

1. Introduction

[2] Geological and paleomagnetic evidence indicate that during at least two Neoproterozoic glacial periods (~630 Ma and ~715 Ma) continental ice sheets flowed into the ocean near the equator [*Kirschvink*, 1992; *Hoffman et al.*, 1998; *Evans*, 2000]. These glacial formations are nearly universally overlain with cap carbonates, which suggests that the glacial periods were immediately followed by extremely hot conditions [*Hoffman et al.*, 1998]. This observation is particularly noteworthy since it is suggestive of strong nonlinearity in global climate, and potentially bistability and hysteresis with respect to changes in greenhouse gas forcing. Indeed, global climate models spanning the full range of complexity do exhibit bistability between a completely ice-covered state and a partially or fully ice-free state [*Sellers*, 1969; *Budyko*, 1969; *Marotzke and Botzet*, 2007; *Voigt and Marotzke*, 2010; *Voigt et al.*, 2011; *Pierrehumbert et al.*, 2011], which is ultimately due to the nonlinearity caused by the difference between the reflectivity of liquid water and ice. Crucially, if Earth were in a globally-glaciated state, silicate weathering would essentially cease, allowing the atmospheric CO_2 concentration to build up to immense values [*Walker et al.*, 1981]. The synthesis of these ideas and observations led to the "Snowball Earth" model for Neoproterozoic glaciations, in which some combination of forcings pushes the climate into a stable state with global coverage of the oceans with ice, which decreases silicate weathering such that atmospheric CO_2 can reach high enough values that the ice-covered climate state can eventually be exited [*Kirschvink*, 1992; *Hoffman et al.*, 1998].

[3] Since the Snowball Earth model was proposed, two important observations have been made that appear to be consistent with it. First, extreme oxygen isotopic anomalies have been observed in sulfate minerals [*Bao et al.*, 2008, 2009] that suggest high CO_2 values, $\mathcal{O}$(0.01–0.1 bar), during and just after the ~630 Ma glaciation. Although these CO_2 values are likely too low to deglaciate a Snowball Earth by

[1]Department of Geophysical Sciences, University of Chicago, Chicago, Illinois, USA.
[2]Max Planck Institute for Meteorology, Hamburg, Germany.

0148-0227/11/2011JD015927

themselves [*Pierrehumbert*, 2004], they would probably be sufficient if the albedo-reducing effects of the aeolian and volcanic dust that are expected during a Snowball Earth event are accounted for [*Abbot and Pierrehumbert*, 2010; *Le Hir et al.*, 2010; *Abbot and Halevy*, 2010]. Second, large Iridium anomalies in cap carbonates in the Eastern Congo Craton [*Bodiselitsch et al.*, 2005] may suggest that the glacial period lasted 3–12 Myr, although this result has not been reproduced elsewhere. Importantly, both of these observations suggest that Neoproterozoic glaciations are associated with strong hysteresis as CO_2 is varied.

[4] Biological evidence, however, paints a somewhat more ambiguous picture for the Snowball model. For example, micropaleontological and molecular clock evidence indicate that photosynthetic eukaryotes thrived both before and immediately after the Snowball episodes [*Knoll*, 1985; *Bosak et al.*, 2011]. Furthermore, the presence of fossil steroids [*Love et al.*, 2009], molecular clock evidence [*Sperling et al.*, 2010], and possible fossils [*Maloof et al.*, 2010] suggest that multiple lineages of sponges, which are complex marine animals, survived both Neoproterozoic glaciations. Taken together, this evidence seems to indicate that some large region of ocean remained ice-free during Neoproterozoic glaciations. While life, perhaps even complex marine life, could survive a Snowball Earth in geothermal refugia [e.g., *Hoffman and Schrag* 2000], we believe it is useful to consider whether alternative models for Neoproterozoic glaciations could explain the physical evidence without requiring a completely ice-covered ocean.

[5] One alternative to the Snowball model is the "Slushball Earth" model, which is also sometimes called the "Oasis" solution, the "soft-Snowball", or the "waterbelt." The Slushball model is based on the fact that it may be possible for ice sheets to grow on tropical continents even if the equatorial ocean remains ice-free [*Hyde et al.*, 2000]. In the Slushball model ice would expand over the ocean down to roughly 25–40° latitude, but the bifurcation in global climate leading to global ice coverage would never occur. Although the Slushball model would naturally explain the survival of marine animal and photosynthetic life through Neoproterozoic glaciations, it appears to be in conflict with some of the physical evidence. Most importantly, the Slushball model allows only weak hysteresis in global climate, associated with the growth of continental ice sheets [*Crowley et al.*, 2001]. In this case by weak we mean specifically that the hysteresis appears to be too small to explain the proxy-CO_2 measurements and the nearly-universal occurrence of cap carbonates. For example, the Slushball climate states in the model of *Liu and Peltier* [2010] occur for CO_2 values of $\mathcal{O}$(100–1000) ppmv. A maximum pCO_2 value of $\mathcal{O}$(1000) ppm is one to two orders of magnitude less than the values indicated by the measurements of *Bao et al.* [2008, 2009] and it is difficult to imagine that massive cap carbonates would be deposited globally at such a low pCO_2 value. Therefore, the Slushball state is qualitatively similar to the Pleistocene glaciations of the last few million years, but more extreme, whereas Neoproterozoic glaciations appear to be qualitatively different phenomena.

[6] The tropical "thin-ice" solution is another model that has been proposed for Neoproterozoic glaciations [*McKay*, 2000; *Pollard and Kasting*, 2005]. In this model the ocean would be ice-covered, but the ice would only be $\mathcal{O}$(1 m) thick in the tropics, which would allow the penetration of photosynthetically active radiation into the ocean below. *Pollard and Kasting* [2005] showed that such a solution is possible in an energy balance climate model if: (1) bare sea ice has high transmissivity and an albedo of 0.4–0.5 as opposed to a higher albedo (≈0.8) of snow covered sea ice, and (2) moisture is exported from the tropics so that sea ice in the tropics is bare and has the corresponding low albedo. In addition to potentially allowing the survival of photosynthetic life through Neoproterozoic glaciations, the thin-ice solution was associated with hysteresis in the *Pollard and Kasting* [2005] model such that pCO_2 must be increased ≈30 times to terminate it. This means that if the thin-ice solution were entered at roughly modern pCO_2 (≈300 ppm), it would be terminated at a pCO_2 of ≈0.01 bar, which is of the order indicated by the work of *Bao et al.* [2008, 2009]. Although the thin-ice solution remains a potentially viable model for Neoproterozoic glaciations, it has not been found in a global climate model so far, and it is the subject of debate whether the parameter regime in the *Pollard and Kasting* [2005] model in which the thin-ice solution exists is physically realistic [*Warren and Brandt*, 2006; *Pollard and Kasting*, 2006].

[7] Many global climate models that have been used to simulate Neoproterozoic glaciations either do not keep track of snow on sea ice or use a small contrast between the albedos of snow and ice [*Pierrehumbert et al.*, 2011]. There are a few examples of simulations of Neoproterozoic glaciations in global climate models in the literature that use a low (~0.4–0.5) bare sea ice albedo [*Chandler and Sohl*, 2000; *Micheels and Montenari*, 2008; *Pierrehumbert et al.*, 2011]. In each of these studies, which utilized different climate models, large series of simulations were performed and thin-ice solutions were not found. For certain climate forcings, however, a very narrow region of open ocean in the tropics was found, with ice at higher latitudes. The sea-ice latitude, the average latitude of the ocean-sea-ice interface, in these cases was 5–15°, which compares with 25–40° in the Slushball model [*Hyde et al.*, 2000].

[8] The possibility of a thin-ice solution [*McKay*, 2000; *Pollard and Kasting*, 2005] or a solution with a very narrow strip of open ocean in the tropics [*Chandler and Sohl*, 2000; *Micheels and Montenari*, 2008; *Pierrehumbert et al.*, 2011] if the bare sea ice albedo is low underscores the crucial role that ice albedo plays in climate modeling of Neoproterozoic glaciations. *Warren et al.* [2002] contains perhaps the most useful review of appropriate ice and snow albedo values in the context of Neoproterozoic glaciations. Based on measurements of sea ice at −5°C reported by *Brandt et al.* [1999, 2005], *Warren et al.* [2002] argue that the appropriate value for the broadband albedo of exposed, non-melting ice formed by freezing seawater during a Neoproterozoic glaciation is 0.47 at temperatures above −23°C. At temperatures below −23°C, NaCl precipitates out of saturated solution as hydrohalite ($NaCl \cdot 2H_2O$ [*Light et al.*, 2009]), which could increase the appropriate albedo to 0.71 [*Warren et al.*, 2002]. Finally, the appropriate albedo for snow covered ice is 0.81 [*Warren et al.*, 2002]. These values suggest that a strong contrast between bare and snow covered ice is appropriate when simulating Neoproterozoic glaciations.

[9] In this paper we will continue the investigation into the effect of a low bare sea ice albedo on climate solutions

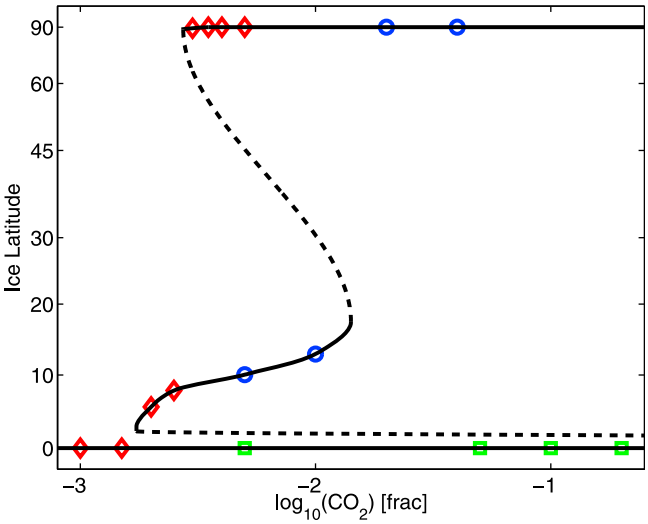

Figure 1. Bifurcation diagram of global climate in the CAM atmospheric global climate model, run as described in section 2. Red diamonds denote simulations initiated from ice-free conditions, blue circles denote simulations initiated from the Jormungand state, and green squares denote simulations initiated from the Snowball state. The ice latitude plotted here is the inverse sine of the global and annual mean open ocean fraction of the equilibrated climate. The numerical burden of calculating the precise positions of the unstable solution branches (separatrices) and bifurcations is prohibitive in CAM, so they have been schematically added to this diagram.

that might be relevant for Neoproterozoic glaciations. Similar to *Chandler and Sohl* [2000], *Micheels and Montenari* [2008], and *Pierrehumbert et al.* [2011], we find that in the global climate models we use, a solution with an extremely low sea-ice latitude occurs when the bare sea ice albedo is low, rather than a thin-ice solution. Significantly, we also find that if the top-of-atmosphere albedo is higher in snow covered than bare sea ice regions, the climate solution with a low sea-ice latitude represents a distinct state of global climate that is separated by bifurcations from the modern state and the Snowball state. Furthermore, if the albedo above snow covered regions is ≈0.7–0.8, this climate state allows for strong hysteresis in global climate, i.e., the state exists at pCO_2 values consistent with *Bao et al.* [2008, 2009]. Since this state is characterized by a thin strip of open ocean that stretches around the planet, snaking back and forth across the equator with the seasonal cycle, we have named it the Jormungand state, after the world serpent and enemy of Thor in Norse mythology. Although the Jormungand state and the Slushball model share the characteristic of a tropical region of open ocean, they are qualitatively different for at least three reasons. First, there are two new bifurcations in global climate and one new unstable state associated with the Jormungand state. Second, the hysteresis associated with the Jormungand state is much larger and is ultimately due to atmospheric dynamics rather than the dynamics of continental ice sheets. Third, the strip of open ocean is much smaller in the Jormungand state than in a Slushball. Our investigation of the Jormungand state in this paper is preliminary, but we believe it is sufficient to demonstrate that the Jormungand state is a plausible model for Neoproterozoic glaciations that deserves further attention.

[10] The outline of this paper is as follows. In section 2 we describe the Jormungand state in atmospheric global climate models. In section 3 we show that it is possible to modify the Budyko-Sellers model so that it produces the Jormungand state. We then use this modified Budyko-Sellers model to study how albedo and heat transport parametrizations of this model affect the Jormungand state. We discuss our results in section 4 and conclude in section 5.

2. The Jormungand State in Atmospheric Global Climate Models

[11] In this section we will begin by describing simulations in a global climate model that produce the Jormungand state. These simulations are performed with the National Center for Atmospheric Research's Community Atmosphere Model v3.1 (CAM [*Collins et al.*, 2004; *McCaa et al.*, 2004]) run at T42 horizontal resolution (2.8° × 2.8°) with 26 vertical levels. They use the idealized configuration described by *Pierrehumbert et al.* [2011]. Specifically, we run the model in aquaplanet mode (no continents) with an ocean mixed layer of depth 50 m, a thermodynamic sea ice scheme, no applied ocean heat transport, no aerosols, and with full diurnal and annual cycles, but a solar constant that is 94% of its modern value and zero eccentricity.

[12] Importantly, bare sea ice has a much lower albedo than snow in CAM. Assuming 40% of incoming light is visible [*Gill*, 1982], we calculate CAM's bare sea-ice broadband albedo is ≈0.45 and snow covered sea-ice broadband albedo is ≈0.79 when the surface temperature is below −1°C [*Collins et al.*, 2004]. These values compare favorably with the measurements discussed by *Warren et al.* [2002], although we should note that the broadband albedo varies depending on atmospheric conditions. The bare sea-ice albedo decreases to 0.38 and the snow covered albedo decreases to 0.66 at 0°C to account for the formation of melt ponds on the ice surface, which have a lower albedo than ice itself [*Collins et al.*, 2004]. There is uncertainty in exactly how much the albedo of melting ice should be reduced, but this effect is fairly small in CAM.

[13] Figure 1 shows a bifurcation diagram of global climate with pCO_2 as the control parameter produced from equilibrated simulations in CAM. Specifically, we plot the ice latitude, or inverse sine of the global and annual mean open ocean fraction, for each equilibrated simulation. This model exhibits three stable global climate states: (1) a warm, ice-free state (ice latitude of 90°), (2) a cold state with ice latitude at 5–15°, and (3) a Snowball state with 100% sea-ice coverage (ice latitude of 0°). As mentioned above, we refer to the nearly ice-covered climate state as a "Jormungand" state, because the open ocean region in this state traces a narrow serpent-like path in a Hovmoller diagram (Figure 2). There is strong hysteresis associated with the Jormungand state, which is to say that the Jormungand state and one or both of the other states are stable for a wide range of pCO_2 (for a volume fraction between approximately 0.00175–0.015, or 1750–15000 ppm). The Jormungand state might exist at a much lower pCO_2, potentially making the hysteresis associated with this state much larger, if a dynamic ocean were

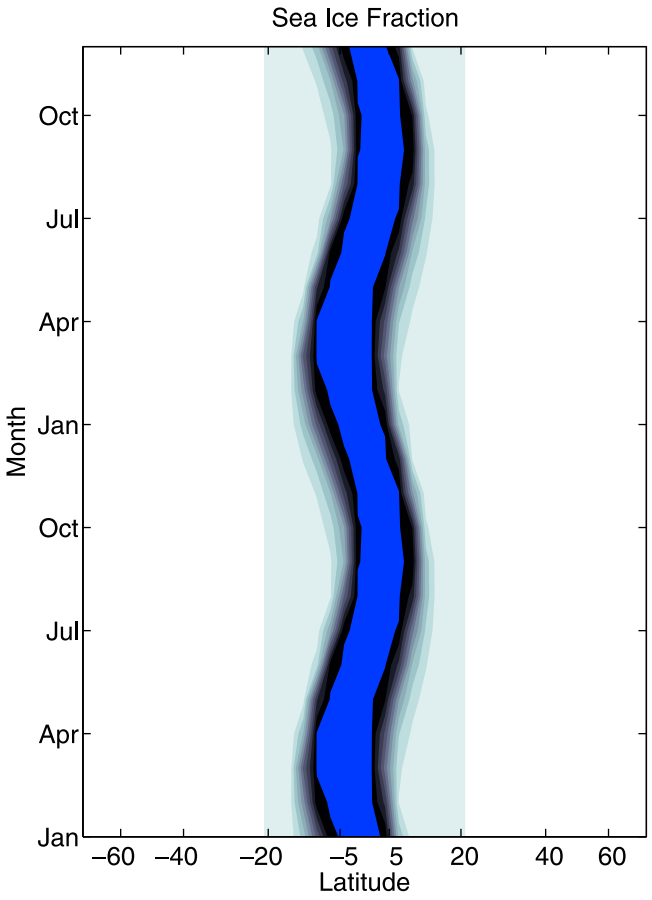

Figure 2. Hovmoller diagram of the zonal mean sea-ice fraction in the Jormungand state with pCO_2 = 2000 ppm. Open ocean is plotted blue and regions of 100% ice coverage are plotted white. Contours at every 10% ice coverage interpolate between these end-members. The Jormungand state is named for the serpent-like weaving of the narrow open ocean region in this diagram.

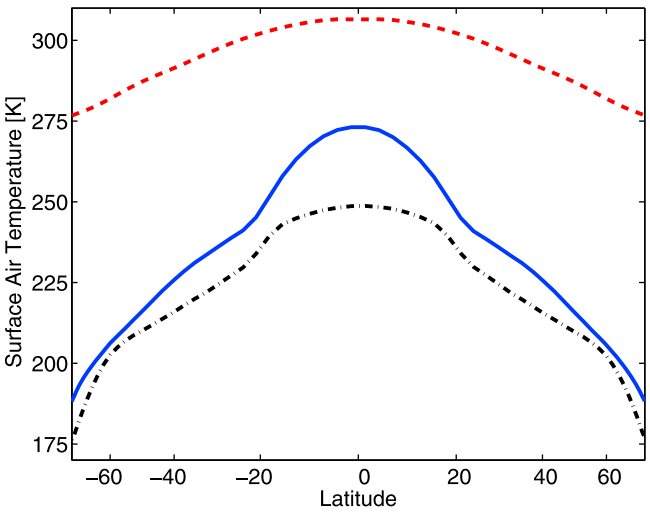

Figure 3. Annual and zonal mean surface air temperature for the ice-free state (red dashed), Jormungand state (blue), and Snowball state (black dash-dotted) with pCO_2 = 5000 ppm.

used rather than a mixed layer with zero ocean heat transport. This is because ocean heat transport plays an important role in stabilizing the ice latitude and preventing it from proceeding equatorward [*Rose and Marshall*, 2009]. Although we run CAM in an idealized configuration here, so we do not consider detailed comparison with data useful, it is important to note that the Jormungand state exists up to a pCO_2 value on the order of those reported by *Bao et al.* [2008, 2009].

[14] The tristability of CAM for a wide range of pCO_2 allows us to directly compare the three global climate states at the same climate forcing (solar forcing, greenhouse gas levels, and surface boundary conditions). While the surface air temperatures of the Jormungand and Snowball states are quite similar in the extratropics (Figure 3), the deep tropics (latitude less than approximately 20°) are 30–35 K warmer in the Jormungand state than in the Snowball state. This raises the near-equatorial surface temperature of the Jormungand state to just above freezing, which allows this state to exist. In contrast, the ice-free state is drastically warmer at all latitudes and has a greatly reduced meridional temperature gradient relative to the Jormungand and Snowball states. It is remarkable that the three states can coexist at the same climate forcing.

[15] Figure 4 shows the annual and zonal mean precipitation minus evaporation ($P - E$) in the ice-free state and the Jormungand state with pCO_2 = 5000 ppm. $P - E$ is roughly two orders of magnitude smaller in the Snowball state, so it is not plotted here. For both the ice-free and Jormungand states the seasonal variation of $P - E$ is small in the tropics due to the large thermal inertia of ocean at the surface there. $P - E$ is proportional to the vertical mean of the convergence of the product of the atmospheric meridional velocity and the specific humidity. The similarity of the shape of the tropical $P - E$ pattern in the ice-free and Jormungand states, combined with the fact that eddy moisture transport is small

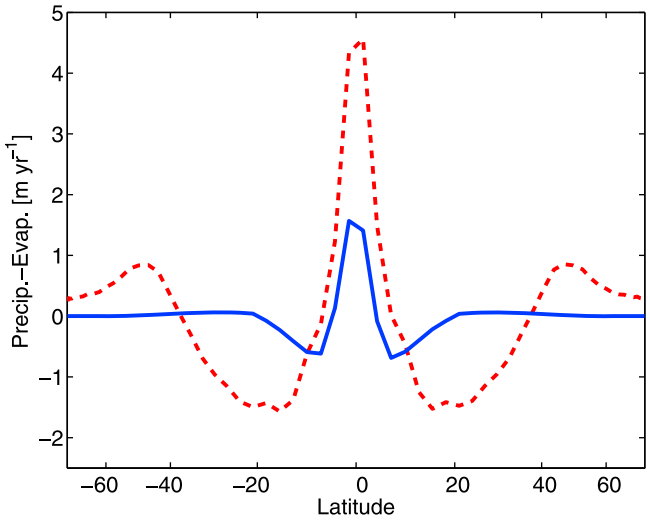

Figure 4. Annual and zonal mean precipitation minus evaporation for the ice-free state (red dashed) and the Jormungand state (blue) with pCO_2 = 5000 ppm.

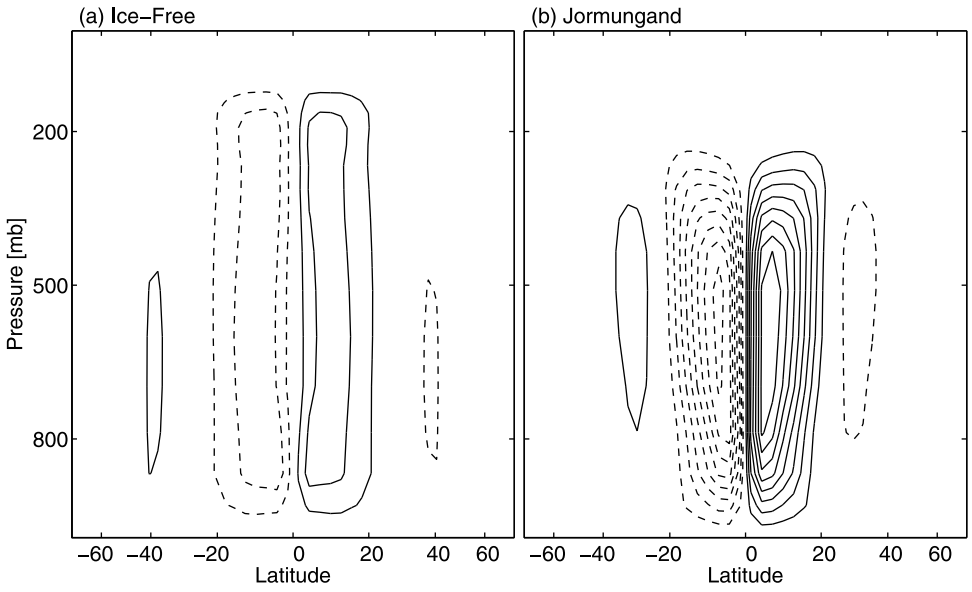

Figure 5. Annual-mean stream function of atmospheric circulation in the (a) ice-free and (b) Jormungand states with $pCO_2 = 5000$ ppm. Contour intervals are 5×10^{10} kg s^{-1}. Positive contours are solid and negative contours are dashed. The zero contour is not plotted.

in the tropics, implies that the pattern of the tropical zonal-mean circulation is broadly similar in these states, which is indeed the case (Figure 5). The reduced magnitude of $P - E$ in the Jormungand state relative to the ice-free state, despite a Hadley circulation that is about four times stronger (Figure 5), is due to the Jormungand state being much colder and drier. In the ice-free climate eddy moisture transport causes $P - E < 0$ up to nearly ≈40° and $P - E$ strongly greater than zero at latitudes higher than ≈40°. In the Jormungand state it is so cold poleward of ≈20° (Figure 3) that eddy moisture transport has a negligible effect on the global $P - E$ pattern compared to the Hadley circulation (Figure 4). $P - E$ peaks at about 6 cm yr^{-1} in the extratropics of the Jormungand state, which, although small, is enough to lead to significant snow coverage over time (Figure 6).

[16] The $P - E$ pattern in the Jormungand state is crucial for the maintenance of the state: wherever annual-mean $P - E > 0$, snow will build up on sea ice, while wherever annual-mean $P - E < 0$, sea ice will be bare (not covered with snow most of the time). Since the tropical maximum in $P - E$ (the inter-tropical convergence zone or ITCZ) is within the ocean strip of the Jormungand state, any sea ice equatorward of about 20° is generally bare in this state (Figure 6). There is an occasional dusting of sea ice within this region with snow, but it generally sublimates within a month. As mentioned above, there is a strong contrast between the bare and snow covered sea ice albedo in CAM (notice that surface temperatures of bare sea ice in the Jormungand state (Figure 3) exceed the threshold of −23°C for hydrohalite formation [*Light et al.*, 2009], so that the bare sea ice albedo used in CAM is appropriate). The effect of this contrast can be seen in the annual and zonal mean top-of-atmosphere albedo in the Jormungand state (Figure 7). Even though there is seasonal ice coverage for latitudes less than 20°, the top-of-atmosphere albedo in this region is between 0.3–0.6. These values represent a mix of seasonally-varying bare sea ice, open ocean, and overlying clouds. Since this region is under the descending branch of the Hadley circulation (Figure 5), it is relatively cloud-free so that the surface albedo dominates the top-of-atmosphere albedo. In contrast, the top-of-atmosphere albedo over the open-ocean region near the equator is much higher than the surface albedo corresponding to open ocean (Figure 7) because the cloudy ITCZ occurs in this region.

[17] The difference in top-of-atmosphere albedo between the bare and snow covered sea ice regions is essential for the existence of the Jormungand state. Since high latitude sea ice is covered with snow, it has a high albedo, so that when the ice latitude is near the pole, the ice-albedo feedback is

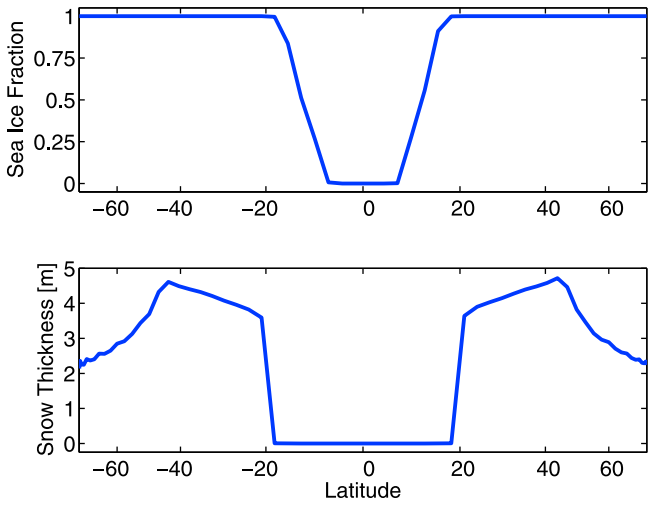

Figure 6. Annual and zonal mean (top) sea-ice fraction and (bottom) snow thickness in the Jormungand state (blue) with $pCO_2 = 5000$ ppm.

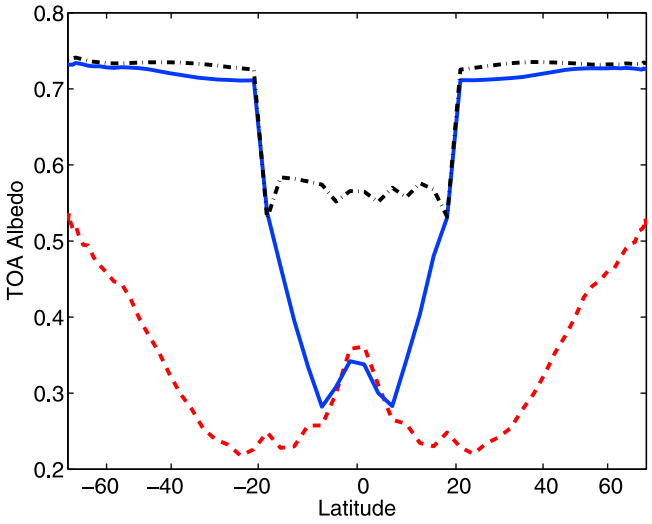

Figure 7. Annual and zonal mean top of the atmosphere (TOA) albedo for the ice-free state (red dashed), Jormungand state (blue), and Snowball state (black dash-dotted) with pCO_2 = 5000 ppm. The albedo plotted here is the ratio of the outgoing to the incident TOA shortwave radiation, calculated only when the incident TOA shortwave radiation exceeds 50 W m^{-2}.

strong. When the ice latitude is near the equator, however, sea ice is bare and the ice-albedo feedback is weak enough that the negative radiation feedback can stabilize global climate in the Jormungand state. This reduction of the strength of the ice-albedo feedback in the tropics allows the ice latitude to stay very near to the equator without actually reaching the equator. Therefore a Jormungand state is a natural outcome of the extension of sea ice into the subtropical "desert" zone as long as bare sea ice has a sufficiently low albedo. The high contrast between the albedo of bare and snow covered sea ice then leads to the co-existence of the stable Jormungand and ice-free states over a significant range of CO_2 concentrations.

[18] We provide a schematic diagram of the interaction of the ocean-ice-snow albedo with atmospheric dynamics that allows the Jormungand state to exist in Figure 8. We expect that thick sea glaciers [*Goodman and Pierrehumbert*, 2003; *Pollard and Kasting*, 2005; *Goodman*, 2006] would develop in the snow covered extratropical regions, although we have not shown that here. It is important to reiterate that it is atmospheric dynamics that set the boundary between high-albedo snow and low-albedo bare sea ice.

[19] As a further test of the proposed mechanism, we consider whether we can induce a Jormungand state in a different model by modifying the sea-ice albedo scheme such that there is a strong contrast between the bare ice and snow albedo. Specifically, we consider the Max Planck Institute's atmospheric model v5.3.02p (ECHAM5) [*Roeckner et al.*, 2003], which does not produce a Jormungand state when it is run at T31 horizontal resolution (3.75° × 3.75°) with 19 vertical levels in the idealized configuration used here [*Pierrehumbert et al.*, 2011]. Since ECHAM5 does not keep track of snow that falls on sea ice when it is not coupled to a dynamical ocean model, the model does not discriminate between the albedo of bare and snow covered sea ice. Instead the sea ice albedo in ECHAM5 is simply 0.75 at −1°C and linearly ramped to 0.55 at 0°C. As a crude way of simulating the effects of the hydrological cycle on sea-ice albedo, we modify ECHAM5 such that sea ice has CAM's snow albedo poleward of 20° latitude and CAM's bare sea-ice albedo equatorward of 20° latitude. The resulting bifurcation diagram of global climate is shown in Figure 9. Importantly, the modifications to the sea-ice albedo scheme do produce a Jormungand state. Furthermore, the Jormungand state in ECHAM5 shows a similar P-E pattern and intensified Hadley cells as in CAM (not shown). The hysteresis associated with the Jormungand state in the modified ECHAM5, however, is smaller than in CAM. This could result from different model atmospheric dynamics, cloud simulation, or the crude representation of the hydrological cycle by the modified sea-ice albedo in ECHAM5. The hysteresis associated with the Snowball state is also much smaller than in CAM. This is likely due to the fact that in CAM the top-of-atmosphere

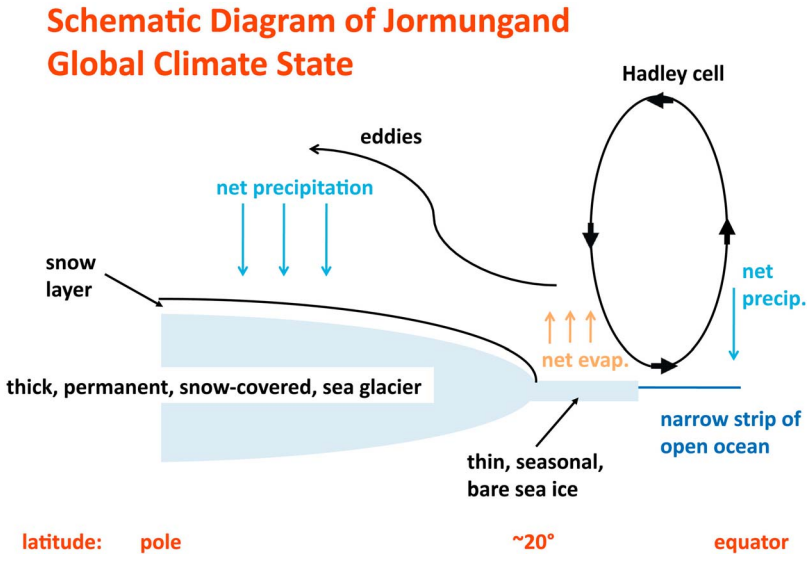

Figure 8. Schematic diagram of the Jormungand global climate state.

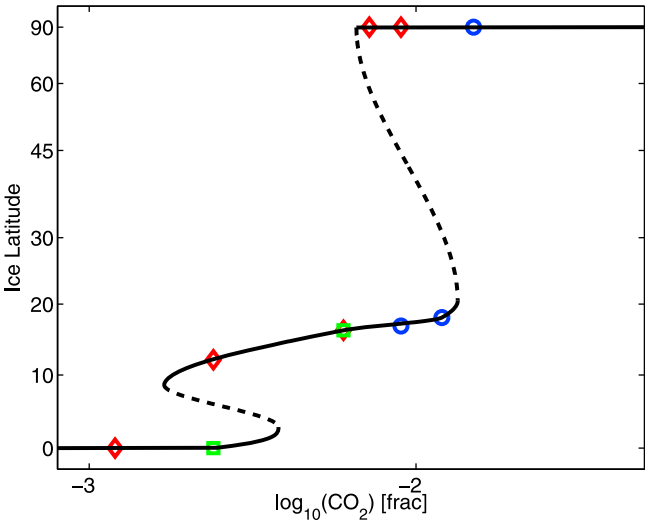

Figure 9. As in Figure 1, but using the ECHAM5 atmospheric global climate model instead of CAM. A modification to the ECHAM5 sea ice scheme, described in section 2, is required to produce this diagram.

albedo in the tropics of the Snowball state is higher than in the partially ice-covered region of the Jormungand state (Figure 7). This probably results from partial (not 100%) and seasonal sea ice coverage in the tropics of the Jormungand state (Figure 2).

3. The Jormungand State in the Budyko-Sellers Model

[20] There are numerous assumptions that go into global climate models that may not be appropriate in climates vastly different from our own (see *Abbot et al.* [2010] for an example). Additionally, there are undoubtedly bugs hidden in the code of these models, which can be mistaken for true physics when one views model results. Therefore, it is useful to complement the results of global climate models with understanding gained from low-order models [*Held*, 2005]. In this light, we here study the Jormungand state using the Budyko-Sellers energy balance model [*Budyko*, 1969; *Sellers*, 1969].

3.1. Review of the Budyko-Sellers Model

[21] Here we briefly review the Budyko-Sellers model [*Budyko*, 1969; *Sellers*, 1969]. Below we will refer to the Budyko-Sellers model as described here as the "standard" Budyko-Sellers model, in order to differentiate it from the "modified" Budyko-Sellers model that we introduce in section 3.2.

[22] At steady state, the fundamental energy balance of the Budyko-Sellers model is given by

$$\frac{Q}{4}S(x)(1-\alpha(T(x))) = A + BT(x) + C\left(T(x)-\overline{T}\right), \quad (1)$$

where Q is the solar constant, $S(x)$ describes the meridional distribution of incoming solar radiation, T is the surface temperature, $A + BT$ is a linearization of the outgoing longwave radiation flux as a function of surface temperature, $C(T(x) - \overline{T})$ is a simple parameterization of the meridional redistribution of heat by the atmosphere and ocean, C is a constant with the same units as B, and x is the sine of the latitude. It is standard to take $x \in [0, 1]$ and to consider only solutions that are symmetric with respect to reflection across the equator. $\alpha(T(x))$ is the albedo, which is generally assumed to have a strong dependence on temperature to simulate the ice-albedo feedback. For example,

$$\alpha(T(x)) = \begin{cases} \alpha_1 & T > T_s \\ \alpha_s & T = T_s \\ \alpha_2 & T < T_s \end{cases}, \quad (2)$$

where α_1 is a low albedo representing open ocean and clouds above it; α_2 is a high albedo representing sea ice, snow, and clouds above it; T_s is the annual-mean surface temperature at which ice forms, i.e., the temperature at the ice latitude, and is generally taken to be −10°C based on observations of the modern climate; and α_s is usually taken to be the arithmetic mean of α_1 and α_2. Note that the subscripts s indicate variables at the ice latitude, rather than at the surface. These variables, such as T_s, are therefore constants that are independent of latitude. Following *North* [1975a, 1975b], we approximate $S(x)$ as

$$S(x) = 1 - \frac{s_2}{2} + \frac{3}{2}s_2x^2, \quad (3)$$

where $s_2 = -0.482$. We can calculate the global mean energy balance by integrating equation (1) from $x = 0$ to $x = 1$

$$\frac{Q}{4}\left(1-\alpha_p(x_s)\right) = A + B\overline{T}, \quad (4)$$

where $\alpha_p(x_s)$, the global mean albedo, is defined by

$$\alpha_p(x_s) = \int_0^1 \alpha(x)S(x)dx = \alpha_1\int_0^{x_s} S(x)dx + \alpha_2\int_{x_s}^1 S(x)dx, \quad (5)$$

where x_s is the sine of the ice latitude. Since we have assumed that $S(x)$ is quadratic (equation (3)), the integrals in equation (5) are easy to compute. If we consider equation (1) at the ice latitude ($x = x_s$), we find

$$\frac{Q}{4}S(x_s)(1-\alpha_s) = A + BT_s + C\left(T_s - \overline{T}\right). \quad (6)$$

We can substitute $\overline{T}$ from equation (4) into equation (6) to find the following relation for A as a function of x_s

$$A(x_s) = \frac{1}{1+\frac{C}{B}}\left(\frac{Q}{4}\left(S(x_s)(1-\alpha_s) + \frac{C}{B}\left(1-\alpha_p(x_s)\right)\right) - (B+C)T_s\right). \quad (7)$$

Equation (7) represents a solution to the Budyko-Sellers model, since it allows us to calculate the ice latitude if we are given A. We will focus on the decrease in A from its current

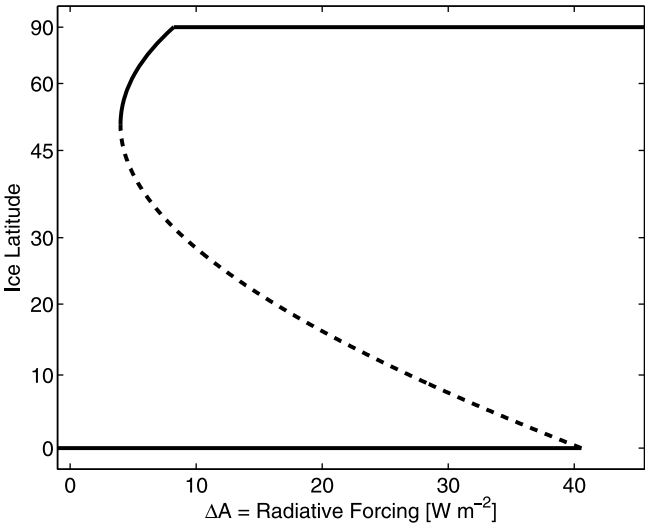

Figure 10. Bifurcation diagram of global climate in the Budyko-Sellers model with Q_0 = 1285 W m^{-2}, A_0 = 210 W m^{-2}, B = 1.5 W m^{-2} K^{-1}, $C = 2.5B$, $\alpha_1 = 0.3$, $\alpha_2 = 0.6$, $T_s = -10$°C, and $s_2 = -0.482$. ΔA is the reduction in outgoing longwave radiative from a standard value ($\Delta A = A_0 - A$) and represents a proxy for changes in greenhouse gas forcing. Solid lines represent stable equilibria and dashed lines represent unstable equilibria.

value, $\Delta A = A_0 - A$, which we can think of as the radiative forcing due to increased optical thickness of the atmosphere (due to increased greenhouse gases, for example) relative to the present.

[23] Roughly following *Roe and Baker* [2010], we can calculate the stability of the equilibria by first noting from equation (7) that

$$\frac{4}{Q}(B+C)\Delta A + BS(x_s)(1-\alpha_s) - C\alpha_p(x_s) = const., \quad (8)$$

so that

$$\frac{4}{Q}(B+C)\delta(\Delta A) + \left(B\frac{\partial S}{\partial x_s}(1-\alpha_s) - C\frac{\partial \alpha_p}{\partial x_s}\right)\delta x_s = 0, \quad (9)$$

which leads to

$$\frac{\delta x_s}{\delta(\Delta A)} = \frac{\frac{4}{Q}(B+C)}{C\frac{\partial \alpha_p}{\partial x_s} - B\frac{\partial S}{\partial x_s}(1-\alpha_s)}. \quad (10)$$

If $\frac{\delta x_s}{\delta(\Delta A)} > 0$ on a steady state solution then reducing the radiative forcing causes the ice latitude to move equatorward, and vice versa, so the state is stable. Similarly when $\frac{\delta x_s}{\delta(\Delta A)} < 0$ the solution is unstable and when $\frac{\delta x_s}{\delta(\Delta A)}$ becomes infinite there is a bifurcation. This is an example of the "slope-stability" theorem, a more general consideration of which can be found in *Cahalan and North* [1979]. Using equation (10) it is easy to show that the solution line is stable for x_s greater than the bifurcation at $0 < x_s < 1$ and unstable for x_s less than this bifurcation (use $\frac{\partial \alpha_p}{\partial x_s} = S(x_s)(\alpha_1 - \alpha_2(x_s))$ from equation (5) and note that s_2 is negative). We show a bifurcation diagram of the standard Budyko-Sellers model in Figure 10, generated using the solution and stability criteria outlined in this section.

3.2. Modifying the Budyko-Sellers Model to Produce the Jormungand State

[24] The Jormungand global climate state depends on the difference between the albedo of snow covered and bare sea ice, which is not incorporated into the standard Budyko-Sellers model. To include this effect we let α_2 take a snow covered value (α_2^s) poleward of a transition latitude and a bare sea ice value (α_2^i) equatorward of this transition latitude. Mathematically, we take

$$\alpha_2 \equiv \alpha_2(x) = \alpha_2^i + \left(\frac{\alpha_2^s - \alpha_2^i}{2}\right)\left(1 + \tanh\left(\frac{x - x_i}{\Delta x_i}\right)\right), \quad (11)$$

where x_i is the sine of the latitude of the transition from bare to snow covered sea ice, and Δx_i is the width (in sine latitude) of the transition region. In a global climate model x_i and Δx_i are set by atmospheric dynamics, but we must impose x_i and Δx_i in the Budyko-Sellers model. We can still use equation (7) to solve the model as long as we recalculate α_s and $\alpha_p(x_s)$ using equation (11).

[25] To calculate stability of the states, we calculate $\frac{\delta x_s}{\delta(\Delta A)}$ using the method described in section 3.1. We find a relation similar to equation (10)

$$\frac{\delta x_s}{\delta(\Delta A)} = \frac{\frac{4}{Q}(B+C)}{BS\frac{\partial \alpha_s}{\partial x_s} + C\frac{\partial \alpha_p}{\partial x_s} - B\frac{\partial S}{\partial x_s}(1-\alpha_s)}. \quad (12)$$

Note that in the standard Budyko-Sellers model $\frac{\partial \alpha_s}{\partial x_s} = 0$, but in the modified Budyko-Sellers model $\frac{\partial \alpha_s}{\partial x_s}$ is nonzero near the ice-snow transition.

[26] Our parameter choices for the modified Budyko-Sellers model are motivated by results from CAM, but ultimately selected so that the modified Budyko-Sellers model bifurcation diagram is similar to that of CAM. The fact that it is possible to obtain a similar bifurcation diagram at all with our simple modification to the model (equation (11)) suggests that our explanation for the Jormungand state is sound. Furthermore, we will subject the model to a sensitivity study (section 3.3) that shows that the behavior we describe is fairly robust, and suggests the qualitative control on the Jormungand state of the physical processes that model parameters represent.

[27] We take $x_i = 0.35$ based on the CAM simulations (section 2) and $\Delta x_i = 0.04$. We choose albedo and ice-snow transition parameters of the modified Budyko-Sellers model to correspond roughly with those produced by CAM (section 2). We also take $\frac{C}{B} = 1.5$, as opposed to $\frac{C}{B} = 2.4$ in the work by *Budyko* [1969] and $\frac{C}{B} = 2.5$ in Figure 10, because meridional heat transport in CAM is relatively inefficient in the Jormungand state (poleward heat transport across 45° of ~2.25 PW (10^{15} W) in the Jormungand state as opposed to ~4.75 PW in the warm state). This is the result of both a strong inversion in the mid and high latitudes, which reduces eddy activity, and extremely cold temperatures in the mid and high latitudes, which reduces moist energy transport. Finally, we let $T_s = 0$°C since this value is more appropriate if the ice

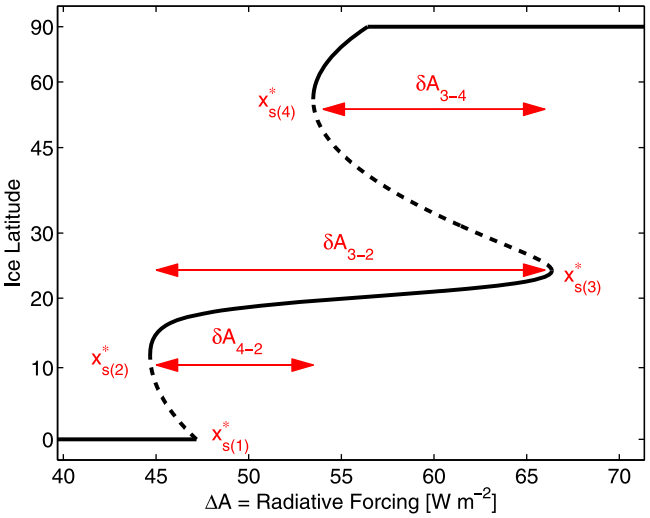

Figure 11. As in Figure 10, but using equation (11) for the snow/ice albedo. All parameters are as in Figure 10 except $\alpha_1 = 0.35$, $\alpha_2^i = 0.45$, $\alpha_2^s = 0.8$, $T_s = 0°C$, $C = 1.5B$, $x_i = 0.35$, and $\Delta x_i = 0.04$. The Jormungand global climate state is the new stable state with an ice latitude between 10–25°. Four bifurcations in global climate exist in the plot. These bifurcations are labeled $x^*_{s(j)}$, where j is an index ranging from one to four with increasing value denoting increasing ice latitude. $\delta A_{j-i} = \Delta A(x^*_{s(j)}) - \Delta A(x^*_{s(i)}) = A(x^*_{s(i)}) - A(x^*_{s(j)})$ represents the difference in radiative forcing values of two respective bifurcations.

latitude is near the equator where the seasonal cycle is small [*Pierrehumbert*, 2005].

[28] We show a bifurcation diagram of the modified Budyko-Sellers model in Figure 11, using equation (12) to calculate the stability of states. The Jormungand state is the new stable state with an ice latitude near, but not at, the equator. Two new bifurcations and a new unstable state accompany the Jormungand state. The model now has four bifurcations, which we label $x^*_{s(j)}$ where j is an index ranging from one to four with increasing value denoting increasing ice latitude.

[29] By design, the bifurcation diagram produced by the modified Budyko-Sellers model is generally similar to that obtained in CAM (Figure 1), which lends confidence to our explanation of the physical mechanism that allows the Jormungand state to exist. There are, however, two significant differences between the bifurcation diagrams. The first major difference is that the formation of even a very small amount of ice in CAM destabilizes the ice-free climate and forces the model into a Jormungand state, whereas the warm climate state in the Budyko-Sellers model is stable until the ice latitude reaches roughly 60°. Since ice cap states are possible in the real climate system, we consider this a deficiency of the CAM simulations that is probably related to the idealized configuration we use. The second major difference is that the Snowball state is much more stable in CAM than in the Budyko-Sellers model, so that a much higher radiative forcing is required to produce the bifurcation through which the Snowball state is lost ($x^*_{s(1)}$) in CAM. As for the ECHAM5 simulations with CAM-like sea-ice albedo (section 2), this results from the tropical top-of-atmosphere albedo being higher in the Snowball state than in the Jormungand state in CAM, which is an effect we do not include in the modified Budyko-Sellers model. We will discuss how these differences might affect the interpretation of our results in section 4.

3.3. Using the Model to Understand the Jormungand State Better

[30] In this section we study the way in which the positions of the four bifurcations of the modified Budyko-Sellers model are affected by changes in model parameters, in order to understand better what controls the behavior of the Jormungand state. We will discuss the ice latitudes at which the bifurcations occur ($x^*_{s(j)}$) and the difference in ΔA between different bifurcations, which we denote δA_{j-i} ($\delta A_{j-i} = \Delta A(x^*_{s(j)}) - \Delta A(x^*_{s(i)}) = A(x^*_{s(i)}) - A(x^*_{s(j)})$). $x^*_{s(j)}$ and δA_{j-i} are drawn schematically on Figure 11. Calculating δA_{j-i} allows us to address the following issues of physical importance. First, δA_{3-2} represents the range in radiative forcing (ΔA) over which the Jormungand state exists. Second, δA_{3-4} is a measure of the hysteresis in radiative forcing associated with the Jormungand state and the warm state. Finally, δA_{4-2} tells us whether the Jormungand state would be accessible to global climate as the CO_2 were decreased starting in the warm state. If $\delta A_{4-2} < 0$, then global climate jumps straight from the warm state to the Snowball state as CO_2 is decreased.

[31] We begin by finding the relations for the bifurcations in the model, which are necessary for calculating δA_{j-i}. The bifurcations in the model occur when $\frac{\delta x_s}{\delta(\Delta A)}$ becomes infinite. Using equation (12) this corresponds to

$$\frac{\partial S}{\partial x_s}(1-\alpha_s(x_s)) - S(x_s)\frac{\partial \alpha_s}{\partial x_s} - \frac{C}{B}\frac{\partial \alpha_p}{\partial x_s} = 0. \tag{13}$$

Note again that in the standard Budyko-Sellers model $\frac{\partial \alpha_s}{\partial x_s} = 0$, but in the modified Budyko-Sellers model $\frac{\partial \alpha_s}{\partial x_s}$ is nonzero near the ice-snow transition. Using equation (13), $\frac{\partial \alpha_p}{\partial x_s} = S(x_s)(\alpha_1 - \alpha_2(x_s))$, and $\alpha_s = \frac{1}{2}(\alpha_1 + \alpha_2(x_s))$, we find

$$\frac{\partial S}{\partial x_s}\left(1 - \frac{1}{2}(\alpha_1 + \alpha_2(x_s))\right) = S(x_s)\left(\frac{C}{B}(\alpha_1 - \alpha_2(x_s)) + \frac{1}{2}\frac{\partial \alpha_2}{\partial x_s}\right). \tag{14}$$

We can make progress solving for the positions of bifurcations 2 and 4 using equation (14) if we assume that these bifurcations occur far enough away from the ice-snow transition latitude that $\frac{\partial \alpha_2}{\partial x_s} \approx 0$. Using this assumption and equation (3), we find that $x^*_{s(2)}$ satisfies the following quadratic relation

$$\frac{3}{2}s_2\left(x^*_{s(2)}\right)^2 - \frac{3s_2(1-\alpha_s)}{\frac{C}{B}\left(\alpha_1 - \alpha_2^i\right)}x^*_{s(2)} + 1 - \frac{1}{2}s_2 = 0. \tag{15}$$

$x^*_{s(4)}$ satisfies a relation equivalent to equation (15) with α_2^s substituted for α_2^i. Physically it is clear that as $\Delta x \to 0$, $x^*_{s(3)} \to x_i$. A perturbative relation can be derived for $x^*_{s(3)}$, but we do not find that it lends much insight. We will solve equation (14) numerically to find the exact positions of all of the bifurcations below.

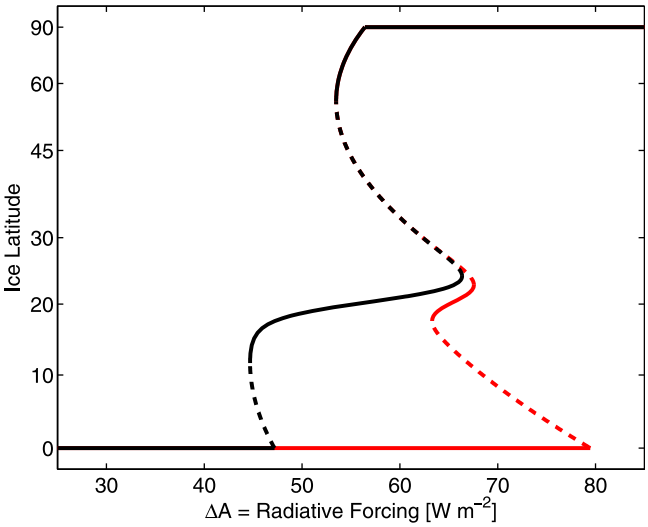

Figure 12. As in Figure 11, with $\alpha_2^i = 0.45$ (black) and with $\alpha_2^i = 0.65$ (red). In the latter case the Jormungand state is not "accessible" if the radiative forcing (ΔA) is increased and decreased through a hysteresis loop between the warm state and the Snowball state.

[32] Using equation (7), we can write the difference in ΔA values between two different bifurcations (δA_{j-i}) as

$$\delta A_{j-i} = \frac{Q/4}{1 + C/B}\left(S\left(x^*_{s(i)}\right)\left(1 - \alpha_s\left(x^*_{s(i)}\right)\right) + \frac{C}{B}\left(1 - \alpha_p\left(x^*_{s(i)}\right)\right) - S\left(x^*_{s(j)}\right)\left(1 - \alpha_s\left(x^*_{s(j)}\right)\right) - \frac{C}{B}\left(1 - \alpha_p\left(x^*_{s(j)}\right)\right)\right), \quad (16)$$

which we will evaluate using the numerical solutions for $x^*_{s(j)}$.

[33] We find that the Jormungand state exists ($\delta A_{3-2} > 0$) and there is hysteresis associated with it if it is accessible ($\delta A_{3-4} > 0$) throughout the physically-relevant parameter regime. For example, as long as the bare sea-ice albedo is less than the snow albedo ($\alpha_2^i < \alpha_2^s$), the Jormungand state exists. The most interesting question relating to the qualitative behavior of the Jormungand state that we can consider using the modified Budyko-Sellers model is whether the Jormungand state is accessible from the warm state by reducing the radiative forcing ($\delta A_{4-2} > 0$).

[34] Accessibility is important because if the Jormungand state has a small basin of attraction and is an interior state to a larger hysteresis loop between the warm state and Snowball state, it will be difficult to find in global climate models and would be less relevant as a model for Neoproterozoic glaciations. One way this might happen is if the top-of-atmosphere albedo in bare sea ice regions (α_2^i) is close to the top-of-atmosphere albedo in snow covered sea ice regions. Figure 12 shows the effect on the global climate bifurcation diagram of increasing α_2^i from 0.45 to 0.65. The Jormungand state is inaccessible from the warm state through reductions in ΔA in the later case, and would likely not be found in a global climate model.

[35] Figure 13 contains diagrams that depict the regions of parameter space of the modified Budyko-Sellers model in which the Jormungand state is accessible ($\delta A_{4-2} > 0$). We focus on variables whose analogs are most likely to differ between global climate models. The main effect of increasing α_2^i is that it makes it easier for the Jormungand state to freeze into the Snowball state, which means that less reduction of radiative forcing is needed to destroy the Jormungand state, implying that $\Delta A(x^*_{s(2)})$ increases and δA_{4-2} decreases (Figure 13).

[36] Making meridional heat transport more efficient by increasing $\frac{C}{B}$ leads to a larger $\Delta A(x^*_{s(4)})$ and a smaller $\Delta A(x^*_{s(2)})$. This can be understood from the fact that $x^*_{s(4)}$ is in a region of net convergence of meridional heat transport while $x^*_{s(2)}$ is in a region of net divergence of meridional heat transport. Increasing the efficiency of meridional heat transport therefore makes it harder to freeze out of the warm state, which means that the warm state is lost at a lower radiative forcing ($\Delta A(x^*_{s(4)})$ decreases). Similar reasoning applies for $x^*_{s(2)}$, yielding significant decreases in δA_{4-2} as $\frac{C}{B}$ is increased (Figure 13).

[37] Decreasing α_1 decreases the global mean albedo (α_p) and the ice-latitude albedo (α_s), and therefore decreases $\Delta A(x^*_{s(j)})$, for all bifurcations (equation (7)). The decrease in α_p is larger the more open ocean is exposed (the more poleward the ice latitude is), which explains why the change in ΔA is larger for the more poleward bifurcations. This, in

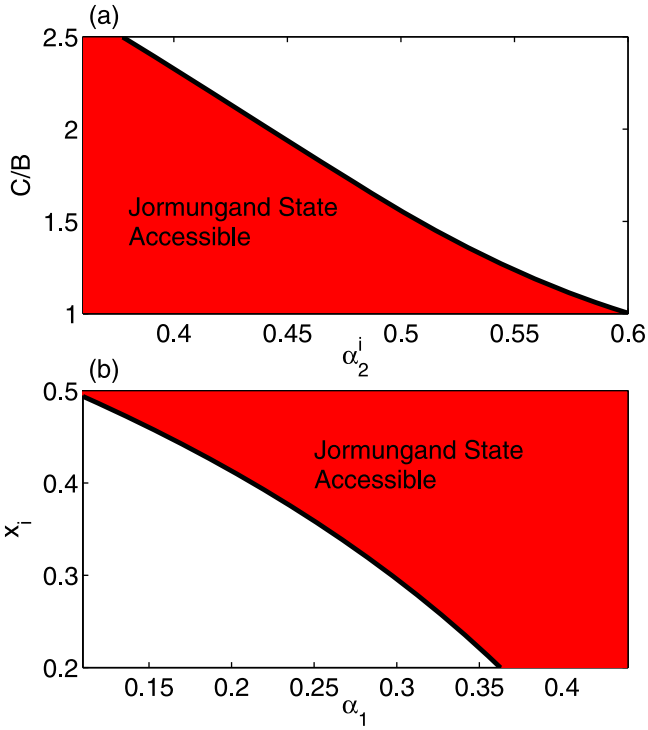

Figure 13. Diagram indicating the region in which $\delta A_{4-2} > 0$ (marked red) as a function of: α_2^i, the bare sea-ice albedo; C/B, a measure of the efficiency of meridional heat transport (see equation (1)); x_i, the sine of the latitude of the transition from bare to snow covered sea ice; and α_1, the top of the atmosphere albedo over open ocean. When $\delta A_{4-2} > 0$, the Jormungand state is "accessible" as the greenhouse gas forcing is varied (see Figure 12).

turn, explains the fact that δA_{4-2} decreases as α_1 decreases (Figure 13).

[38] When x_i is decreased, $x^*_{s(2)}$ is close enough to the reduced x_i (within a few times Δx_i), that $\alpha_2(x^*_{s(2)})$ increases. Since changes in insolation with latitude are minimal in the tropics, this increase in albedo at the bifurcation that destroys the Jormungand state and forces global climate into the Snowball state makes it easier for this bifurcation to occur. This, in turn, increases $\Delta A(x^*_{s(2)})$, and decreases δA_{4-2} (Figure 13).

4. Discussion

[39] We begin the discussion with a qualitative description of the way in which the Jormungand state could serve as a model for Neoproterozoic glaciations. Suppose Earth starts with a high CO_2 concentration to balance the reduced Neoproterozoic insolation, so that the climate is warm and either ice-free or with a small amount of sea ice near the poles. For some reason the CO_2, or some other greenhouse gas, is reduced and the ice latitude starts to decrease. We leave this point vague intentionally since the reasons for the initiation of Neoproterozoic glaciations are still poorly understood [*Pierrehumbert et al.*, 2011]. Eventually the system reaches a bifurcation and the ice latitude rushes toward the equator. Once the ice latitude reaches about 20–30°, however, it enters the subtropical "desert" band. This means that atmospheric circulation ensures that the sea ice is generally bare and the atmosphere is less cloudy than in other regions, so that the top-of-atmosphere albedo is fairly low in this region. At this point it becomes more difficult for the ice latitude to proceed further equatorward, since the ice-albedo feedback is severely weakened, and the system enters a Jormungand state. Since the Jormungand state is cold and comparatively dry, silicate weathering is greatly reduced. Silicate weathering is additionally reduced by the fact that, according to geological evidence, ice sheets cover large areas of continents in the tropics. The CO_2 concentration cannot decrease any further as a result, and the climate never enters a Snowball state. At this point the CO_2 starts to increase, although this increase is slow since the ocean can equilibrate with the atmosphere and seafloor weathering can occur. The strong hysteresis associated with the Jormungand state (Figure 1) allows the CO_2 to build up to $\mathcal{O}$(0.01 bar) during presumably $\mathcal{O}(10^6$–$10^7)$ years, allowing consistency with geological observations. The growth of land glaciers would be fairly easy in the Jormungand state, since the thin tropical strip of open ocean would provide an ample supply for precipitation. Eventually, the CO_2 builds up to high enough levels that the Jormungand state disappears and global climate returns violently to the ice-free solution, at which time the cap carbonates are deposited.

[40] Various aspects of the geological and geochemical story given in the last paragraph require further elaboration that is beyond the scope of the current work. For example, a study similar to that of *Le Hir et al.* [2008], which could constrain the rate of atmospheric CO_2 increase in a Jormungand state, would be useful for determining the expected lifetime of a Jormungand state for comparison with geochronological data. Additionally, a study of how high pCO_2 needs to be in the aftermath of a glacial event would be helpful for determining the viability of a Jormungand state as a model for Neoproterozoic glaciations. Finally, an ocean geochemical model could be used to determine whether the ocean can become sufficiently anoxic away from the small strip of open ocean in the tropics to form the iron and iron-manganese deposits found in some Neoproterozoic glacial sediments [*Hoffman and Li*, 2009].

[41] The Jormungand and Slushball models for Neoproterozoic glaciations share the characteristic of a region of open ocean in the tropics, but they are different in a number of important ways. First, the region of open ocean in the Jormungand state is much thinner (ice latitude of 5–15° as opposed to 25–40°). Second, the hysteresis as greenhouse gas levels are varied associated with the Jormungand state is potentially much larger than that associated with the Slushball. Any hysteresis in the Slushball model is caused by the growth of continental ice sheets, which would grow in the Jormungand model as well. The hysteresis associated with the Jormungand state that we have found (e.g., Figure 1) would therefore add to any hysteresis associated with the growth of continental ice sheets. Finally, the Slushball model requires continents, but, as we have shown here, the Jormungand state can occur even in atmospheric global climate models run in aquaplanet mode. This point underlines the different physics involved in producing a Jormungand state and a Slushball.

[42] Although the idealized configuration (aquaplanet, mixed layer ocean, no ocean heat transport) we used in the atmospheric global climate model simulations presented here is important for understanding physical behavior, one might wonder what the effects of using more realistic Neoproterozoic boundary conditions might be. Preliminary investigation in both the CAM and ECHAM5 models suggests that the Jormungand state is possible for a range of continental configurations. Additionally, both *Chandler and Sohl* [2000] and *Micheels and Montenari* [2008] find low ice-latitude states that may be examples of the Jormungand state using Neoproterozoic boundary conditions and a parameterization of ocean heat transport. If the mechanism discussed here causes the low ice-latitude states in those studies, this suggests that the existence of the Jormungand state is fairly robust to changes in the details of ocean simulation and continental configuration.

[43] Coupled global climate model simulations described in recently submitted work appears to further support the idea that the Jormungand state can exist with a dynamical ocean and realistic continents (J. Yang et al., The initiation of modern "soft Snowball" and "hard Snowball" climates in CCSM3. Part I: The influence of solar luminosity, CO_2 concentration and the sea-ice/snow albedo parameterization; Part II: Climate dynamic feedbacks, submitted to *Journal of Climate*, 2011, hereinafter referred to as Yang et al., submitted manuscript, 2011a and 2011b, respectively). Yang et al. (submitted manuscript, 2011a, 2011b) use CCSM3, NCAR's coupled ocean-atmosphere climate dynamics model with thermodynamic-dynamic sea ice, run with modern boundary conditions. CCSM3 uses the same version of CAM to simulate atmospheric dynamics as we do and has sea ice and snow albedos similar to those in the CAM simulations shown here. At different CO_2 levels, some of the simulations of Yang et al. (submitted manuscript, 2011a, 2011b) equilibrate with an ice latitude of $\mathcal{O}(10°)$ and others with an ice latitude greater than $\mathcal{O}(40°)$, but solutions with an ice latitude

between ≈10–40° were not found. Additionally, Yang et al. (submitted manuscript, 2011a, 2011b) found bistability of global climate between nearly ice-covered states and states with a smaller ice cap. Taken together, this suggests that the nearly ice-covered CCSM3 solutions found by Yang et al. (submitted manuscript, 2011a, 2011b) may represent the Jormungand state, although further investigation of the specific mechanism that allows these low ice-latitude solutions is needed. If Yang et al. (submitted manuscript, 2011a, 2011b) have found the Jormungand state, then their work is further evidence that ocean dynamics and realistic continents do not necessarily destroy the Jormungand state in a climate model. A point of interest in future investigations of the Jormungand state in coupled global climate models is the amount of hysteresis associated with the Jormungand state in such models.

[44] The effects of thick, flowing "sea glaciers" [*Goodman and Pierrehumbert*, 2003; *Pollard and Kasting*, 2005; *Goodman*, 2006] on the Jormungand state should be considered in future work. It is possible, for example, that flowing sea glaciers could close off the open water region near the equator in the Jormungand state. Calculations, however, suggest that the equatorward flow rate is not fast enough to penetrate far into the tropical ablation region for at least some tropical open water solutions [*Goodman and Pierrehumbert*, 2003]. An additional process not included in previous sea glacier models is the possibility for large-scale collapse of sea glaciers when they enter ablation regions, similar to ice shelve collapse on the Antarctic peninsula linked to surface meltwater [*Scambos et al.*, 2000; *van den Broeke*, 2005]. This process might further decrease the likelihood that sea glacier flow destroys a Jormungand state.

[45] The interaction of snow albedo with the seasonal cycle can lead to climate adjustment times of up to ≈100 years [*Mengel et al.*, 1988]. Additionally, in CAM at least, the Snowball state is more strongly stable than the Jormungand state and exists over the entire CO_2 over which the Jormungand state exists. This might cause worry that climate noise could cause the Jormungand state to transition to the Snowball state (see *Lee and North* [1995] for an example of this type of behavior for a small ice cap). To try to ensure that the examples of the Jormungand state we found in CAM are not artifacts of slow adjustment and are stable to reasonable climate noise, we ran the model for 200–300 years after it settled into the Jormungand state. There was no systematic trend in sea ice coverage or surface temperature throughout these extended runs, but we cannot completely rule out the possibility of a transition to the Snowball or ice-free state on longer timescales.

[46] The results from the modified Budyko-Sellers model may help us understand why the Jormungand state has been found in some global climate models, but not in others. First, these results imply that it is likely that the Jormungand state exists in any global climate model that has even a small contrast between the bare and snow covered sea ice albedo, although it may be inaccessible by only varying radiative forcing and therefore may be difficult to find. The Budyko-Sellers model also shows that other factors such as the albedo over open ocean may be important for determining whether the Jormungand state is accessible in a global climate model. This albedo is mainly determined by cloud cover, and could vary significantly between different models given the uncertainty associated with cloud simulation [e.g., *Cess et al.*, 1990, 1996; *Soden and Held*, 2006].

[47] We have shown how the Budyko-Sellers model can be modified to produce an additional stable state in global climate, the Jormungand state, so that the model exhibits three total states in global climate. We note that this is different from the tristability in global climate discussed by *Rose and Marshall* [2009] and *Ferreira et al.* [2011], for whom the intermediate climate state has a small ice cap near the pole stabilized by the convergence of ocean heat transport. A simple way to produce such tristability, with a small ice cap, in an energy balance model is to model the convergence of meridional heat transport as diffusive rather than using the non-local parameterization in equation (1) [*North*, 1975a, 1984]. It is possible that if we switched our parameterization of meridional heat transport to that of *North* [1975a, 1984], the warm state branch of our bifurcation diagram (Figure 11) would split into a small ice cap state and an ice-free state in some parameter regime. There would therefore be four stable global climate states in this case. Similarly, if we included a parameterization of ocean heat transport or a dynamic ocean in our CAM simulations, it is likely that we would find an additional stable state with a small ice cap like that of *Rose and Marshall* [2009] and *Ferreira et al.* [2011].

[48] As mentioned in section 3.2, we chose a fairly low value of $\frac{C}{B}$ because meridional heat transport is significantly reduced in the Jormungand state. While a low value of $\frac{C}{B}$ is reasonable for the Jormungand state, it is probably not reasonable for the warm state. This represents a limitation on the usefulness of our analysis with respect to $x^*_{s(4)}$, the most poleward bifurcation. It would be possible to develop a model with different values of $\frac{C}{B}$ in different regimes, but at some point such modifications to a simple model render it no longer simple and therefore far less useful. In any case, we still believe that the physical insight gained from section 3.3 is useful for guiding the use of more complex models, which are, in many cases, ultimately a better tool for investigating quantitative questions.

[49] A limitation of the modified Budyko-Sellers model that we have developed here is that it produces a Snowball climate state that disappears at a much lower radiative forcing than in more complex models (compare Figure 11 with *Pierrehumbert* [2004, 2005], *Le Hir et al.* [2007], *Abbot and Pierrehumbert* [2010], *Pierrehumbert et al.* [2011], and *Hu et al.* [2011]). We do not consider this a major problem for this paper, since the bifurcation through which the Snowball state is lost, $x^*_{s(1)}$, is not the focus of this work. We do, however, suggest careful consideration of this issue if the modified Budyko-Sellers model is used in the future to study issues related to the Snowball climate state. In any case the proper simulation of the termination of a Snowball state is likely too complex for the Budyko-Sellers model to provide relevant insight given the importance of clouds [*Le Hir et al.*, 2007; *Abbot and Pierrehumbert*, 2010; *Pierrehumbert et al.*, 2011] and dust [*Abbot and Pierrehumbert*, 2010; *Le Hir et al.*, 2010; *Abbot and Halevy*, 2010] for this process.

5. Conclusions

[50] The main conclusions of this work can be summarized as follows.

[51] 1. We have shown that a new state of global climate, the Jormungand state, is possible in atmospheric global climate models. This state is nearly, but not completely, ice-covered (ice latitude of 5–15°) and exhibits hysteresis as greenhouse gas levels are varied. Both of these properties make the Jormungand state a potential model for Neoproterozoic glaciations.

[52] 2. We find that the Jormungand state occurs in models with a low enough bare sea-ice albedo that there is a strong contrast between the albedo of bare and snow covered sea ice. The Jormungand state is entered when the sea-ice latitude propagates into the robust subtropical "desert" region caused by the descent of the Hadley cell, in which it becomes bare. The top-of-atmosphere albedo above sea ice is much lower in this region than at higher latitudes because bare sea ice is exposed and the atmosphere is relatively less cloudy.

[53] 3. When we modify the "ice" albedo in the Budyko-Sellers energy balance model such that there is a difference between bare and snow covered ice, it produces the Jormungand state. Additionally, the modified Budyko-Sellers model produces a global climate bifurcation diagram that is similar to those of atmospheric global climate models that produce the Jormungand state. This lends confidence to our physical explanation of the maintenance of the Jormungand state.

[54] **Acknowledgments.** We thank J. Amundson, P. Hoffman, F. MacDonald, D. Notz, R. Pierrehumbert, E. Sperling, M. Silber, and S. Warren for conversations or comments on early versions of this manuscript. We thank J. Kasting, G. North, B. Rose, and an anonymous reviewer for thoughtful reviews. D.S.A. was supported by the T. C. Chamberlin Fellowship of the University of Chicago and the Canadian Institute for Advanced Research. This work was supported in part by the Max Planck society. The ECHAM5 simulations were performed at the German Climate Computing Center (DKRZ) in Hamburg, Germany.

References

Abbot, D. S., and I. Halevy (2010), Dust aerosol important for snowball Earth deglaciation, *J. Clim.*, *23*(15), 4121–4132, doi:10.1175/2010JCLI3378.1.

Abbot, D. S., and R. T. Pierrehumbert (2010), Mudball: Surface dust and Snowball Earth deglaciation, *J. Geophys. Res.*, *115*, D03104, doi:10.1029/2009JD012007.

Abbot, D. S., I. Eisenman, and R. T. Pierrehumbert (2010), The importance of ice vertical resolution for Snowball climate and deglaciation, *J. Clim.*, *23*(22), 6100–6109, doi:10.1175/2010JCLI3693.1.

Bao, H., I. Fairchild, P. Wynn, and C. Spotl (2009), Stretching the envelope of past surface environments: Neoproterozoic glacial lakes from Svalbard, *Science*, *323*(5910), 119–122, doi:10.1126/science.1165373.

Bao, H. M., J. R. Lyons, and C. M. Zhou (2008), Triple oxygen isotope evidence for elevated CO_2 levels after a Neoproterozoic glaciation, *Nature*, *453*(7194), 504–506, doi:10.1038/nature06959.

Bodiselitsch, B., C. Koeberl, S. Master, and W. U. Reimold (2005), Estimating duration and intensity of Neoproterozoic Snowball glaciations from Ir anomalies, *Science*, *308*(5719), 239–242, doi:10.1126/science.1104657.

Bosak, T., J. G. Lahr, S. B. Pruss, F. A. Macdonald, L. Dalton, and E. Matys (2011), Surviving the Sturtian Snowball Earth, *Earth Planet. Sci. Lett.*, in press.

Brandt, R., C. S. Roesler, and S. G. Warren (1999), Spectral albedo, absorptance, and transmittance of Antarctic sea ice, paper presented at Fifth Conference on Polar Meteorology and Oceanography, Am. Meteorol. Soc., Dallas, Tex., 10–15 Jan.

Brandt, R., S. Warren, A. Worby, and T. Grenfell (2005), Surface albedo of the Antarctic sea ice zone, *J. Clim.*, *18*(17), 3606–3622.

Budyko, M. I. (1969), The effect of solar radiation variations on the climate of the Earth, *Tellus*, *21*(5), 611–619.

Cahalan, R., and G. North (1979), Stability theorem for energy-balance climate models, *J. Atmos. Sci.*, *36*(7), 1178–1188.

Cess, R. D., et al. (1990), Intercomparison and interpretation of cloud-climate feedback processes in 19 atmospheric general circulation models, *J. Geophys. Res.*, *95*(D10), 16,601–16,615.

Cess, R. D., et al. (1996), Cloud feedback in atmospheric general circulation models: An update, *J. Geophys. Res.*, *101*(D8), 12,791–12,794.

Chandler, M., and L. Sohl (2000), Climate forcings and the initiation of low-latitude ice sheets during the Neoproterozoic Varanger glacial interval, *J. Geophys. Res.*, *105*(D16), 20,737–20,756.

Collins, W. D., et al. (2004), Description of the NCAR Community Atmosphere Model (CAM 3.0), *Tech. Note NCAR/TN-464+STR*, 214 pp., Natl. Cent. for Atmos. Res., Boulder, Colo.

Crowley, T. J., W. T. Hyde, and W. R. Peltier (2001), CO_2 levels required for deglaciation of a "Near-Snowball" Earth, *Geophys. Res. Lett.*, *28*(2), 283–286.

Evans, D. A. D. (2000), Stratigraphic, geochronological, and paleomagnetic constraints upon the Neoproterozoic climatic paradox, *Am. J. Sci.*, *300*(5), 347–433.

Ferreira, D., J. Marshall, and B. Rose (2011), Climate determinism revisited: Multiple equilibria in a complex climate model, *J. Clim.*, *24*(4), 992–1012, doi:10.1175/2010JCLI3580.1.

Gill, A. E. (1982), *Atmosphere-Ocean Dynamics*, 662 pp., Academic, San Diego, Calif.

Goodman, J. C. (2006), Through thick and thin: Marine and meteoric ice in a "Snowball Earth" climate, *Geophys. Res. Lett.*, *33*, L16701, doi:10.1029/2006GL026840.

Goodman, J. C., and R. T. Pierrehumbert (2003), Glacial flow of floating marine ice in "Snowball Earth," *J. Geophys. Res.*, *108*(C10), 3308, doi:10.1029/2002JC001471.

Held, I. M. (2005), The gap between simulation and understanding in climate modeling, *Bull. Am. Meteorol. Soc.*, *86*(11), 1609–1614, doi:10.1175/BAMS-86-11-1609.

Hoffman, P. F., and Z.-X. Li (2009), A palaeogeographic context for Neoproterozoic glaciation, *Palaeogeogr., Palaeoclimatol., Palaeoecol.*, *277*, 158–172.

Hoffman, P. F., and D. P. Schrag (2000), Snowball Earth, *Sci. Am.*, *282*(1), 68–75.

Hoffman, P. F., A. J. Kaufman, G. P. Halverson, and D. P. Schrag (1998), A Neoproterozoic snowball Earth, *Science*, *281*(5381), 1342–1346.

Hu, Y., J. Yang, F. Ding, and W. R. Peltier (2011), Model-dependence of the CO_2 threshold for melting the hard Snowball Earth, *Clim. Past*, *7*(1), 17–25, doi:10.5194/cp-7-17-2011.

Hyde, W. T., T. J. Crowley, S. K. Baum, and W. R. Peltier (2000), Neoproterozoic "Snowball Earth" simulations with a coupled climate/ice-sheet model, *Nature*, *405*(6785), 425–429.

Kirschvink, J. (1992), Late Proterozoic low-latitude global glaciation: The snowball Earth, in *The Proterozoic Biosphere: A Multidisciplinary Study*, edited by J. Schopf and C. Klein, pp. 51–52, Cambridge Univ. Press, New York.

Knoll, A. (1985), The early evolution of eukaryotes: A geological perspective, *Science*, *227*(5057), 57–59.

Le Hir, G., G. Ramstein, Y. Donnadieu, and R. T. Pierrehumbert (2007), Investigating plausible mechanisms to trigger a deglaciation from a hard snowball Earth, *C. R. Geosci.*, *339*(3–4), 274–287, doi:10.1016/j.crte.2006.09.002.

Le Hir, G., G. Ramstein, Y. Donnadieu, and Y. Godderis (2008), Scenario for the evolution of atmospheric pCO_2 during a snowball Earth, *Geology*, *36*(1), 47–50.

Le Hir, G., Y. Donnadieu, G. Krinner, and G. Ramstein (2010), Toward the snowball earth deglaciation, *Clim. Dyn.*, *35*(2–3), 285–297, doi:10.1007/s00382-010-0748-8.

Lee, W., and G. North (1995), Small ice cap instability in the presence of fluctuations, *Clim. Dyn.*, *11*(4), 242–246.

Light, B., R. E. Brandt, and S. G. Warren (2009), Hydrohalite in cold sea ice: Laboratory observations of single crystals, surface accumulations, and migration rates under a temperature gradient, with application to "Snowball Earth," *J. Geophys. Res.*, *114*, C07018, doi:10.1029/2008JC005211.

Liu, Y., and W. R. Peltier (2010), A carbon cycle coupled climate model of Neoproterozoic glaciation: Influence of continental configuration on the formation of a "soft snowball," *J. Geophys. Res.*, *115*, D17111, doi:10.1029/2009JD013082.

Love, G. D., et al. (2009), Fossil steroids record the appearance of Demospongiae during the Cryogenian period, *Nature*, *457*(7230), 718–722, doi:10.1038/nature07673.

Maloof, A. C., C. V. Rose, R. Beach, B. M. Samuels, C. C. Calmet, D. H. Erwin, G. R. Poirier, N. Yao, and F. J. Simons (2010), Possible animal-body fossils in pre-Marinoan limestones from South Australia, *Nat. Geosci.*, *3*(9), 653–659, doi:10.1038/ngeo934.

Marotzke, J., and M. Botzet (2007), Present-day and ice-covered equilibrium states in a comprehensive climate model, *Geophys. Res. Lett.*, *34*, L16704, doi:10.1029/2006GL028880.

McCaa, J., M. Rothstein, B. Eaton, J. Rosinski, E. Kluzek, and M. Vertenstein (2004), User's Guide to the NCAR Community Atmosphere Model (CAM 3.0), user's manual, Natl. Cent. for Atmos. Res., Boulder, Colo. [Available at http://www.ccsm.ucar.edu/models/atm-cam/docs/usersguide/.]

McKay, C. (2000), Thickness of tropical ice and photosynthesis on a snowball Earth, *Geophys. Res. Lett.*, *27*(14), 2153–2156.

Mengel, J., D. Short, and G. North (1988), Seasonal snowline instability in an energy balance model, *Clim. Dyn.*, *2*, 127–131.

Micheels, A., and M. Montenari (2008), A snowball Earth versus a slushball Earth: Results from Neoproterozoic climate modeling sensitivity experiments, *Geosphere*, *4*(2), 401–410, doi:10.1130/GES00098.1.

North, G. (1975a), Analytical solution to a simple climate model with diffusive heat transport, *J. Atmos. Sci.*, *32*(7), 1301–1307.

North, G. R. (1975b), Theory of energy-balance climate models, *J. Atmos. Sci.*, *32*(11), 2033–2043.

North, G. R. (1984), The small ice cap instability in diffusive climate models, *J. Atmos. Sci.*, *41*(23), 3390–3395.

Pierrehumbert, R. T. (2004), High levels of atmospheric carbon dioxide necessary for the termination of global glaciation, *Nature*, *429*(6992), 646–649, doi:10.1038/nature02640.

Pierrehumbert, R. T. (2005), Climate dynamics of a hard snowball Earth, *J. Geophys. Res.*, *110*, D01111, doi:10.1029/2004JD005162.

Pierrehumbert, R. T., D. S. Abbot, A. Voigt, and D. Koll (2011), Climate of the neoproterozoic, *Annu. Rev. Earth Planet. Sci.*, *39*, 417–460, doi:10.1146/annurev-earth-040809-152447.

Pollard, D., and J. F. Kasting (2005), Snowball Earth: A thin-ice solution with flowing sea glaciers, *J. Geophys. Res.*, *110*, C07010, doi:10.1029/2004JC002525.

Pollard, D., and J. F. Kasting (2006), Reply to comment by Stephen G. Warren and Richard E. Brandt on "Snowball Earth: A thin-ice solution with flowing sea glaciers," *J. Geophys. Res.*, *111*, C09017, doi:10.1029/2006JC003488.

Roe, G. H., and M. B. Baker (2010), Notes on a catastrophe: A feedback analysis of snowball Earth, *J. Clim.*, *23*(17), 4694–4703, doi:10.1175/2010JCLI3545.1.

Roeckner, E., et al. (2003), The atmospheric general circulation model ECHAM5, part I: Model description, technical report, Max Planck Inst. for Meteorol., Hamburg, Germany.

Rose, B. E. J., and J. Marshall (2009), Ocean heat transport, sea ice, and multiple climate states: Insights from energy balance models, *J. Atmos. Sci.*, *66*(9), 2828–2843, doi:10.1175/2009JAS3039.1.

Scambos, T., C. Hulbe, M. Fahnestock, and J. Bohlander (2000), The link between climate warming and break-up of ice shelves in the Antarctic Peninsula, *J. Glaciol.*, *46*(154), 516–530.

Sellers, W. D. (1969), A global climate model based on the energy balance of the Earth-atmosphere system, *J. Appl. Meteorol.*, *8*, 392–400.

Soden, B. J., and I. M. Held (2006), An assessment of climate feedbacks in coupled ocean-atmosphere models, *J. Clim.*, *19*(14), 3354–3360.

Sperling, E. A., J. M. Robinson, D. Pisani, and K. J. Peterson (2010), Where's the glass? Biomarkers, molecular clocks, and microRNAs suggest a 200-Myr missing Precambrian fossil record of siliceous sponge spicules, *Geobiology*, *8*(1), 24–36, doi:10.1111/j.1472-4669.2009.00225.x.

van den Broeke, M. (2005), Strong surface melting preceded collapse of antarctic peninsula ice shelf, *Geophys. Res. Lett.*, *32*, L12815, doi:10.1029/2005GL023247.

Voigt, A., and J. Marotzke (2010), The transition from the present-day climate to a modern Snowball Earth, *Clim. Dyn.*, *35*(5), 887–905, doi:10.1007/s00382-009-0633-5.

Voigt, A., D. S. Abbot, R. T. Pierrehumbert, and J. Marotzke (2011), Initiation of a Marinoan Snowball Earth in a state-of-the-art atmosphere-ocean general circulation model, *Clim. Past*, *7*, 249–263, doi:10.5194/cp-7-249-2011.

Walker, J. C. G., P. B. Hays, and J. F. Kasting (1981), A negative feedback mechanism for the long-term stabilization of Earths surface-temperature, *J. Geophys. Res.*, *86*(C10), 9776–9782.

Warren, S. G., and R. E. Brandt (2006), Comment on "Snowball Earth: A thin-ice solution with flowing sea glaciers" by David Pollard and James F. Kasting, *J. Geophys. Res.*, *111*, C09016, doi:10.1029/2005JC003411.

Warren, S. G., R. E. Brandt, T. C. Grenfell, and C. P. McKay (2002), Snowball earth: Ice thickness on the tropical ocean, *J. Geophys. Res.*, *107*(C10), 3167, doi:10.1029/2001JC001123.

D. S. Abbot and D. Koll, Department of Geophysical Sciences, University of Chicago, Chicago, IL 60637, USA. (abbot@uchicago.edu)

A. Voigt, Max Planck Institute for Meteorology, Bundesstr. 53, D-20146 Hamburg, Germany.